Neurotherapeutics (2018) 15:216–232
https://doi.org/10.1007/s13311-017-0591-2

ORIGINAL ARTICLE

iTRAQ-Based Quantitative Proteomics Reveals the New Evidence Base for Traumatic Brain Injury Treated with Targeted Temperature Management

Shi-Xiang Cheng[1] · Zhong-Wei Xu[2] · Tai-Long Yi[1] · Hong-Tao Sun[1] · Cheng Yang[1] · Ze-Qi Yu[1] · Xiao-Sa Yang[1] · Xiao-Han Jin[2] · Yue Tu[1] · Sai Zhang[1]

Published online: 15 December 2017

Abstract

This study aimed to investigate the effects of targeted temperature management (TTM) modulation on traumatic brain injury (TBI) and the involved mechanisms using quantitative proteomics technology. SH-SY5Y and HT-22 cells were subjected to moderate stretch injury using the cell injury controller (CIC), followed by incubation at TTM (mild hypothermia, 32°C), or normothermia (37°C). The real-time morphological changes, cell cycle phase distribution, death, and cell viability were evaluated. Moderate TBI was produced by the controlled cortical impactor (CCI), and the effects of TTM on the neurological damage, neurodegeneration, cerebrovascular histopathology, and behavioral outcome were determined *in vivo*. Results showed that TTM treatment prevented TBI-induced neuronal necrosis in the brain, achieved a substantial reduction in neuronal death both *in vitro* and *in vivo*, reduced cortical lesion volume and neuronal loss, attenuated cerebrovascular histopathological damage, brain edema, and improved behavioral outcome. Using an iTRAQ proteomics approach, proteins that were significantly associated with TTM in experimental TBI were identified. Importantly, changes in four candidate molecules (plasminogen [PLG], antithrombin III [AT III], fibrinogen gamma chain [FGG], transthyretin [TTR]) were verified using TBI rat brain tissues and TBI human cerebrospinal fluid (CSF) samples. This study is one of the first to investigate the neuroprotective effects of TTM on the proteome of human and experimental models of TBI, providing an overall landscape of the TBI brain proteome and a scientific foundation for further assessment of candidate molecules associated with TTM for the promotion of reparative strategies post-TBI.

Keywords Targeted temperature management · Traumatic brain injury · Proteomics · Isobaric tags for relative and absolute quantitation · Cerebrospinal fluid

Introduction

Traumatic brain injury (TBI) remains a major health-care problem worldwide, which is accompanied with high fatality and disability for children and adults [1]. In China, the mortality rate of severe TBI patients is 21.8% according to the Chinese Head Trauma Databank (CHTDB) [2], but these studies of morbidity, mortality, and disability do not take the large number of mild TBI events into consideration for which patients are not hospitalized but only suffer from non-specific symptoms such as headache [3]. For the common and potential devastating effects of TBI, improved early diagnostic methods and treatment strategies to prevent the diverse and complex nature of the pathological processes activated by TBI are critical in the clinical setting, posing major challenges for neurological research.

Shi-Xiang Cheng, Zhong-Wei Xu, Tai-Long Yi contributed equally to this work and should be considered co-first authors.

✉ Shi-Xiang Cheng
shixiangcheng@vip.126.com

✉ Yue Tu
ytumail@vip.126.com

✉ Sai Zhang
zhangsai718@vip.126.com

[1] Tianjin Key Laboratory of Neurotrauma Repair, Institute of Traumatic Brain Injury and Neuroscience, Center for Neurology and Neurosurgery of Affiliated Hospital, Logistics University of Chinese People's Armed Police Force (PAP), Tianjin, China

[2] Central Laboratory of Logistics University of Chinese People's Armed Police Force (PAP), Tianjin, China

In 2011, five international critical care societies recommended replacing the term "therapeutic hypothermia" with "targeted temperature management (TTM)" to emphasize the importance of defining a complete temperature profile [4]. Growing evidence suggests that there are multiple pathways in the cascade of brain injury after TBI, while TTM acts via several mechanisms that have a protective effect against brain injury by promoting neuronal sprouting [5], alleviating inflammation [6], inhibiting necroptosis [7, 8], reducing brain oxygen consumption, excitotoxicity, blood–brain barrier (BBB) disruption and chemical-induced seizures, and inhibiting oxidative stress and cell death [9–11].

There have been various proposals of the mechanisms by which TTM attenuates TBI, including reduction of cerebral metabolic rate of oxygen, cerebral glucose demand, and excitotoxicity in the acute phase, inhibition of inflammation, BBB disruption in the sub-acute phase, and modulation of axonal injury in the chronic phase post-TBI [12], but the translation of these positive data into clinical applications has proven to be controversial. Several large multi-center clinical trials did not show a significant cerebroprotective effect [13, 14], most likely due to the poor understanding of TBI, which reflects the complex, multifactorial nature of cellular responses. Therefore, there is an urgent need for consistent support by key physiological parameters to improve the selection of the candidates during TTM [13].

Recently, neuroproteomics has become a prominent method to assess post-TBI conditions, and plays an increasing role in TBI biomarker discovery [15]. Furthermore, there has been a rapid development of quantitative protein expression technologies, including iTRAQ combined with liquid chromatography (LC) and tandem mass spectrometry (MS/MS), which can construct data-driven systems biology models of TBI by high-throughput data sets, thereby increasing the possibility of identifying less abundant proteins [16]. In the present study, we applied iTRAQ followed by LTQ Orbitrap Velos protein identification and bioinformatics analysis to determine the changes of differentially expressed proteins, identify potential biomarkers associated with TTM, and elucidate the possible role of TTM in the molecular pathways following TBI.

Materials and Methods

Cell Culture, Stretch Injury, and Temperature Modulation

Human neuroblastoma cells (SH-SY5Y) and mouse hippocampal cells (HT-22) were obtained from American Type Culture Collection (ATCC) and maintained in Dulbecco's modified Eagle's medium (Gibco, Waltham, MA, USA) supplemented with 10% fetal bovine serum (Gibco) and 1% penicillin/streptomycin in a humidified atmosphere of 5% CO_2 at 37°C. Cells were randomly divided into 4 groups: 1) injury + normothermia; 2) injury + TTM; 3) uninjured + normothermia; and 4) uninjured + TTM. Cells were seeded at 1×10^5/ml in Bioflex culture plates (FlexCell International, Burlington, NC, USA). For the injury groups, cells were subjected to moderate stretch injury with the cell injury controller II (CIC; Custom Design & Fabrication, Richmond, VA, USA), which uses a controlled pulse of compressed nitrogen gas to transiently deform the silastic membrane and to achieve a predetermined degree of stretch [17]. The parameters for the moderate stretch injury were set at 28 psi with a 50-ms duration, resulting in 10.2-psi peak pressure at the well. Uninjured cells served as controls. Temperature was changed immediately following injury by placing the Bioflex plates in temperature-controlled incubators that were maintained at 32°C (TTM) or 37°C (normothermia) for 6 h. The cells were then routinely harvested. The temperature of 32°C was selected based on previous studies [18–20].

Flow Cytometry and Digital Holographic Microscopy (DHM) Assays

Cells were collected by trypsinization, washed with ice-cold phosphate-buffered saline (PBS), and centrifuged at 200 g for 5 min at 4°C. After vortexing, cells were re-suspended in 70% ethanol, and then stored at 4°C overnight. Cell suspensions were centrifuged at 200 g for 5 min, washed once in ice-cold PBS, and then incubated for 1 h at room temperature in 1 ml of 50 μg/ml of propidium iodine (PI) solution containing 250 μg/ml of DNase-free RNase. The DNA content of cells was immediately measured using a FACSCalibur (BD Biosciences, San Jose, CA, USA) and the proportion of cells within the sub-G_1, G_0/G_1, S, and G_2/M phases were analyzed with the FCS Express software (Version 3; De Novo Software, Los Angeles, CA, USA).

The digital holographic microscope (HoloMonitor M4; Phase Holographic Imaging, Lund, Sweden), placed in an incubator, was used to record 3-dimensional information of injured cells after exposure to hypothermia or normothermia. Digital photos were taken at 12-min intervals for 6 h and time-lapse movies were constructed.

Cell Viability and Cell Death Assays

For cell viability assay, cells were harvested with 0.05% trypsin and re-suspended in PBS. The cell suspensions were assayed using 0.4% trypan blue (Sigma-Aldrich, St. Louis, MO, USA) with the automated Countess System (Life Technologies, Waltham, MA, USA), according to the manufacturer's instructions.

For cell death assay, PI (Sigma-Aldrich) was added at a final concentration of 1 μg/ml and cells were incubated for 15 min at room temperature. On each slide, 5 fields were chosen randomly, and the mean number of PI-positive cells

was calculated. Additionally, Annexin V/PI staining was performed using the Annexin V/PI Detection Kit (BD Pharmingen, San Jose, CA, USA) according to the manufacturer's instructions. Briefly, the cell suspension was incubated with 5 μl Annexin V–fluorescein isothiocyanate and 10 μl PI for 30 min at room temperature in the dark, followed by cytometric analysis. All experiments were performed in triplicate.

Study Design of Animal Models

A total of 160 adult male Sprague Dawley rats (mean body weight 300–350 g) were obtained from the Laboratory Animal Center of the Academy of Military Medical Sciences (Beijing, China) and housed at 20°C to 25°C and 50 ± 5% humidity with *ad libitum* access to food and water and a 12-h light/dark cycle. All surgical and behavioral procedures were done in accordance with the rules and regulations of the Institutional Animal Care and Use Committee of Logistics University of PAP, and complied with the Guide for the Care and Use of Laboratory Animals. Cortical contusion impact (CCI)-induced rate mortality of moderate TBI is usually 10% or less, whereas the mortality rate of this experiment was about 4%. All the deaths of all groups were filled up. Animal groups included: 1) sham + TTM; 2) sham + normothermia; 3) CCI + TTM; and 4) CCI + normothermia (n = 40 per group). The study design is presented in Fig. S1. The study consisted of 2 stages: 1) 6 rats/group, regional cerebral blood flow (rCBF) test, modified neurological severity score (mNSS; for 3 days), and magnetic resonance imaging (MRI; for 4 days) were performed 1 d after CCI, and MWM was performed 11 d after CCI (for continuous 7 d); and 2) 1 day after CCI, the rats were sacrificed for the measurement of the following parameters, with 4 rats/group: lesion volume, brain water content, BBB integrity, histology, Fluoro-Jade C (FJC) staining, immunofluorescence, and Western blotting. In addition, 6 rats per group were subjected to the iTRAQ assay.

Cortical Contusion Impact Injury

The experimental TBI method used in this study was performed using an electric cortical contusion impactor device (eCCI-6.3; Custom Design & Fabrication), as described previously with minor modifications [21]. This model is a predominately focal TBI model [22]. Rats were anesthetized with a nitrous oxide/oxygen mixture (70%/30%) containing 1.4% isoflurane delivered by nose cone. A midline scalp incision was made to expose the skull under sterile conditions. A craniotomy (4 mm in diameter) was performed over the right parietal–temporal cortex at 4.0 mm posterior to the bregma and 3.0 mm lateral from the midline. A 3-mm flat-tipped impactor was placed on the dural surface at a 20° angle, and a brain injury of moderate severity was performed with an impact velocity of 5 m/s, impact depth of 2 mm, and impact dwell time of 200 ms. After impact, the bone was replaced and fixed using bone wax, and the incision was closed with absorbable sutures. Sham-operated animals underwent all surgical craniotomy procedures except for the CCI injury, in order to serve as uninjured controls.

Temperature Manipulations

Temperature manipulation was initiated 30 min after CCI or sham surgery. Core body temperature was continuously monitored with rectal temperature probes. TTM was induced with a hypothermia therapy apparatus (HEMA, Shenzhen, China) by applying an ice blanket over the dorsum of prone rats until a body temperature of 32 ± 0.5°C was achieved. The temperature of 32°C for TTM was chosen according to previous studies in rats [23, 24]. A similar degree of hypothermia is recommended by the American Association of Neurological Surgeons Guidelines for the management of severe TBI [25]. After 6 h of TTM, the rats were allowed to gradually rewarm back to their baseline temperature (37 ± 0.5°C) during a 1-h period using heating lamps. Normothermic animals were maintained at normal baseline temperature following CCI induction. Sham-operated animals received normothermia treatment identical to the normothermia CCI animals.

MRI

T2-weighted MRI scanning was performed using a clinical 3.0-Tesla MRI scanner (Siemens, Erlanger, Germany) equipped with a rat RF coil (50 mm; Chengguang Medical Technologies, Shanghai, China), which was used to visualize lesions following CCI. Briefly, at 1 to 4 days post-CCI, rats (n = 6 in each group) were anesthetized as described above and placed in a prone position with their heads in the rat RF coil. T2-weighted images were acquired using a 2-dimensional rapid acquisition with relaxation enhancement (RARE) sequence with the following parameters: repetition time (TR) = 4000 ms; echo time (TE) = 75 ms; (RARE) factor = 10; field of view (FOV)= 19.2 × 19.2 mm; matrix size = 320 × 320; number of slices = 20; slice thickness = 2 mm.

rCBF

The rCBF in the cerebral cortex of animals was measured by laser Doppler flowmetry (Perimed Periflux 5010; Perimed, Järfälla, Sweden). After 24 h of CCI, rats (n = 6 in each group) were anesthetized as described above and laid in a prone position. The laser probe was placed over the skull in the right middle cerebral artery distribution (centered at 4.0 mm posterior to the bregma and 3.0 mm lateral from the midline). The region to be scanned was 4 × 4 mm.

Lesion Volume Assessment

After 24 h of CCI, animals (n = 4 in each group) were anesthetized as described above and sacrificed by cervical dislocation. Brains were removed for the following lesion volume assessment. For each animal, six 500-μm-thick coronal sections that spanned across a total distance of 3 mm were obtained and stained with cresyl violet (Sigma-Aldrich) for analysis. Contralateral (left hemisphere) and ipsilateral (right hemisphere) substructure volumes were calculated based on stereological methods, as previously described [26]. Volume of tissue loss for each substructure was calculated by subtracting the ipsilateral volume from the contralateral volume.

Determination of Brain Water Content

Cerebral edema was evaluated by water content of the brain tissue at 24 h after CCI (n = 4 in each group), using wet-to-dry weight ratio [27]. Following sacrifice, the brain parenchyma (after discarding the olfactory bulb and cerebellum) was removed and divided into 2 cerebral hemispheres along the midline: ipsilateral (right) and contralateral (left). The cerebrum samples were immediately weighted to obtain the wet weight (WW), and then dried for 24 h at 110°C using a drying oven to obtain the dry weight (DW). The water content was calculated based on the following formula: water content (%) = (WW – DW) / WW × 100%.

Evaluation of BBB Integrity

The integrity of the BBB was determined by assessing the Evans blue (EB) dye extravasation, as described previously [28]. At 23 h post-CCI, rats were anesthetized with an overdose of isoflurane (5%), then injected with 2% solution of EB dye (Sigma-Aldrich) at a dose of 4 ml/kg via the caudal vein, and then allowed to circulate for 1 h prior to sacrifice. Rats were transcardially perfused with saline through the left ventricle until colorless perfusion was achieved. Following sacrifice, the brain was removed, weighted, homogenized in formamide (3 μl/mg), and incubated at room temperature for 48 h. After centrifugation, the supernatant was collected and the optical density was measured at 625 nm, which was used to determine the relative amount of EB dye.

Specimen Preparation and Histological Analysis

After 24 h of CCI, animals (n = 4 in each group) were anesthetized as described above. Cardiac regions exposing by thoracotomy, and left ventricular cannulation of the ascending aorta was performed. Rats were perfused with 200 ml buffered saline solution to flush the blood followed by 700 ml of 4% paraformaldehyde in a (pH 7.2–7.4) for perfusion fixation. Following complete perfusion, rats were decapitated and whole brains were extracted. Whole-brain tissues were fixed overnight in fresh 4% paraformaldehyde at 4°C and then embedded in paraffin. Sections were dried overnight at room temperature, stained using hematoxylin and eosin, and observed by bright-field microscopy (Leica Microsystems, Erlangen, Germany).

FJC Staining

FJC (Chemicon, Temecula, CA, USA) was used as a marker to specially stain degenerating neurons following TBI, as previously described [29]. Briefly, the slides were rinsed in distilled water for 2 min, incubated in descending concentrations of ethanol (5 min in 100%, and 2 min each in 70% and 30%), and then immersed in 0.06% $KMnO_4$ for 10 min. After rinsing in water, sections were exposed to 0.001% FJC in the dark for 30 min, and 4',6-diamidino-2-phenylindole (DAPI) was used to stain the nuclei. Subsequently, slides were rinsed 3 times in water and dried at 37°C. The mean number of FJC-positive cells was counted by a blinded observer in 3 coronal sections in 5 random, non-repeated visual fields covering the injured cortex site using the inverted Leica DMI 4000B fluorescence microscope.

Immunofluorescence Histochemistry and Confocal Imaging

Specimens were dewaxed and hydrated, treated with 2% rabbit serum (Epitomics, Burlingame, CA, USA), and incubated with the primary antibody overnight at 4°C. Then, slides were washed 3 times with a washing buffer for 5 min each and stained with the secondary antibody for 30 min in darkness at 37°C. After washing with 10 μM PBS 3 times for a total of 15 min, DAPI was used to stain the nuclei. Finally, sections were sealed and imaged on a TCS SP8 laser scanning confocol microscope (Leica Microsystems). In this regard, the following primary antibodies produced in rabbit and obtained from Abcam (Cambridge, MA, USA), including anti-antithrombin III (AT III, ab126598), anti-plasminogen (Plg, ab154560), anti-fibrinogen γ chain (Fgg, ab96532), and anti-transthyretin (TTR, ab78548), were diluted 1:100 in PBS. The secondary antibody was fluorescein isothiocyanate-labeled goat antirabbit antibody (1:400; KPL Gaithersburg, MD, USA).

Behavioral Testing

mNSS

mNSS was used to evaluate neurological function deficits in rats (n = 20 in each group) at 2 days after CCI, which is a composite of motor, sensory, balance, and reflex tests. The

maximum points are 6, 2, 6, and 4, respectively. Thus, a higher score indicates more severe neurological dysfunction (13–18 designates severe, 7–12 moderate, and 1–6 mild) [30].

Morris Water Maze

Starting on post-injury day (PID) 11, the Morris water maze (MWM) test was performed by a blinded observer to test the spatial learning ability of rats, as previously described [31]. Briefly, the rats (n = 20 in each group) were placed in a circular tank containing opaque water and were trained to find a submerged platform. Acquisition training consisted of a total of 28 trials, given 4 trials per day for consecutive days [postinjury day (PID) 11–17]. For each trial, the rat was randomly placed at 1 of 4 starting positions. The escape latency time to reach the platform and the swimming path were recorded by the automatic tracking system (Zhenghua Biologic Apparatus, Huaibei, China).

Protein Digestion and Isobaric Tag Labeling

The brain tissues just covering the injury or the corresponding part of the sham rats were snap frozen in liquid nitrogen and homogenized in urea solution (8 M urea, 50 mM ammonium bicarbonate, and 5 mM iodoacetamide). Equal amount of protein (n = 6 in each group) were pooled. Samples were diluted 4 times before digested with trypsin at a 1:50 ratio overnight. The digested peptides were filtered with a microcon (Cat. 42410; Millipore, Billerica, MA, USA), desalted, and vacuum dried. Dried peptides were labeled with 4-plex iTRAQ reagent kits (Applied Biosystems, Foster City, CA, USA) in triethylammonium bicarbonate buffer (pH 8.5) at room temperature for 1 h. Samples of sham + 37°C, sham + 32°C, CCI + 37°C, and CCI + 32°C were labeled as 114, 115, 116, and 117 iTRAQ tags, respectively. The labeled peptides were desalted by stagetips and then dried [32].

LC-MS/MS Analysis

The labeled peptides were dissolved in phase A (3% acetonitrile (ACN), pH was adjusted to 10.0 by NH_3•H_2O) and mixed equally. Then the mixed peptides were loaded onto an L-3000 HPLC System (Rigol, Beijing, China) and separated with a Durashell RP column (3 μm, 700 Å, 250 mm × 4.6 mm i.d.; Agela, Wilmington, DE, USA) using the following gradient: 1% to 6% B (98% ACN, pH 10.0), 8 min; 6% to 21% B, 40 min; 21% to 35% B, 28 min; 35% to 95% B, 8 min; 95% B, 6 min. The flow rate was 800 μl/min and 35 fractions were collected. All the samples were dried under vacuum.

The separated peptides were re-suspended in 1% acetonitrile, 0.5 (v/v) formic acid (FA) and loaded onto a nanoflow HPLC system (NannoAcquity LC; Waters, Milford, MA, USA) equipped with a 15-cm C_{18}-reversed phase column (75 mm inner diameter, 3 μm, Dr Maisch GmbH Reprosil-Pur 120 C_{18}-AQ resin) with a 60 min gradient from 2% to 60% acetonitrile in 0.5% acetic acid at a flow of 250 nl/min. The separated peptides were injected into an LTQ-Orbitrap Velos mass spectrometer (Thermo Scientific, San Jose, CA, USA) in data-dependent mode. The MS parameters were as follows: ion transfer tube was at 250°C and the voltage of the ion source at 1.8 kV. The MS1 scan range was m/z 300 to 1600 with resolution of 30,000. The top-20 intense peaks charged from 2 to 7 were acquired with high energy collision dissociation (HCD). Normalized collision energy was 45%. The automatic gain control (AGC) was 3×10^4 with a maximum ion accumulation time of 250 ms and a signal intensity threshold of 500. Dynamic exclusion time was 30 s. HCD fragmentation ions were detected in the orbitrap at a resolution setting of 7.5×10^3.

Biological Function Analysis

The raw files were analyzed with MaxQuant (version 1.5.3.28) and MS/MS spectra were searched against the Swiss-Prot Rattus norvegicus reference protein database Uniprot (release 2015_08, 7928 query number) and quantified by iTRAQ 4-plex report ions. The target–decoy based strategy was used to control the peptide and protein false discovery rate (FDR). Fully tryptic digestion and up to 2 missed cleavages were selected. Precursor ion peaks were searched with an initial mass tolerance of 20 ppm and fragmented ion peaks were searched with an initial mass tolerance of 0.1 Da. The fixed modifications of carbamidomethylation (+57.021465), iTRAQ 4-plex (K), and iTRAQ 4-plex (N-term) were specified and the variable modification was methionine oxidation (+15.99492). The FDR of peptides and proteins was set to 0.01.

Gene Ontology (GO) annotation analysis was performed using DAVID (https://david.ncifcrf.gov/) [33, 34], and the *Rattus norvegicus* was selected as the background and species. The significance was determined with slight modifications as recommended by the authors of DAVID according to the Benajmini correction of $p < 0.05$. Ingenuity Pathway Analysis software (IPA, version 14400082; Ingenuity Systems, Redwood City, CA, USA) was used to assign the signaling pathway analysis for these altering proteins. The protein–protein interaction (PPI) network was generated using the CluePedia plugin of the Cytoscape version 3.2.1.

Human Subject Characteristics and Cerebrospinal Fluid Collection

Twenty people with TBI (7 mild TBI: Glasgow Coma Scale [GCS] score 13–15; 5 moderate TBI: GCS score 9–12; 8 severe TBI: GCS score 3–8) were prospectively enrolled at the neuro-intensive care unit of the Neurosurgery and Neurology Hospital of PAP, Tianjin, China between 2015 and 2016. The study was approved by the Institutional

Review Board at the Logistics University of PAP (PJHEC-2016-A8) and informed consent was obtained for collection of the cerebrospinal fluid (CSF). The inclusion criteria were age between 18 and 65 years, a history of confirmed closed TBI within 6 h before admission, and abnormal images confirmed by computed tomography scan of the brain, including skull fracture, contusion, or hematoma. Patients with severely combined injury, pre-existing medical conditions, for instance cardiac arrest or penetrating TBI, and pregnant or breast-feeding women were excluded.

All treatment procedures were standardized, step-wise, based on current guidelines [20, 25], for instance head elevation, ventilation control, sedation and analgesia, hyperosmolar therapy, and extraventricular drainage (EVD) catheter for intracranial pressure monitoring and management, as previously described [35], to maintain internal environment and intracranial pressure. In this study, patients with severe TBI who were randomized to the TTM group were cooled to 32°C with the use of cooling blankets and maintained for 24 h. Thereafter, the patients were rewarmed slowly at no greater than 0.5°C every 4 h to prevent rebound intracranial hypertension. Patients with severe TBI randomized to normothermia and other patients with moderate or mild TBI were maintained at 37°C during the entire study period.

For patients with moderate or severe TBI, CSF was obtained directly from EVD catheters, which were placed as a standard of care. For patients with mild TBI, CSF was collected via lumbar puncture. CSF was acquired at separate time points: mild TBI (PID 1), moderate TBI (PID 1), and severe TBI (PID 1 and 3). A volume of 2 ml per sample was collected, centrifuged at 4°C for 10 min, and stored at –80°C until analysis.

Western Blotting and Enzyme-Linked Immunosorbent Assay

Western Blotting

CSF samples (10 μl) were separated by 10% sodium dodecyl sulfate polyacrylamid gel electrophoresis and transferred to nitrocellulose (NC) membranes. The membranes were blocked by 10% non-fat milk and incubated with the primary antibodies (PLG, AT III, FGG, and TTR; Abcam, Cambridge, MA, USA) at a dilution of 1:1000 overnight at 4°C. After washing 3 times with PBS/0.1% Tween-20, membranes were incubated at room temperature for 1 h with horseradish peroxidase-conjugated secondary antibody (IgG at 1:10,000 dilution; KPL). The membranes were washed as mentioned above.

Enzyme-Linked Immunosorbent Assays

CSF samples were diluted and measured by enzyme-linked immunosorbent assay (ELISA) kits [Cloud-Clone (USCN), Houston, TX, USA] for quantitative analysis of AT III (SEC313Hu), PLG (SEB236Hu), FGG (SEC477Hu), and TTR (SEA726Hu) levels according to the manufacturer's protocols. Briefly, the plates were coated with detecting antibody and washed with a buffered solution. Samples and known control solutions were then applied to individual wells. Absorbance was quantified using a microplate spectrophotometer (Multiskan GO; Thermo Scientific), and concentrations of samples were calculated based on standard curves generated from known solutions.

Small Interfering RNA and Cell Viability

For the knockdown of *PLG*, *AT III*, and *FGG* genes, PLG (103869), AT III (118569), and FGG (121886) sequences were obtained from Thermo Fisher. Knockdown was then performed in HT-22 cells using Lipofectamine 2000 (Invitrogen, Carlsbad, CA, USA), according to the manufacturer's instructions. The cell-damage assessment and TTM assay were conducted at 24 h after cell transfection. The effectiveness of gene knockdown was verified by Western blot. Cell viability was measured 12 h after cell damage, using the CellTiter 96 AQueous One solution Cell Proliferation Assay kit (Promega, Madison, WI, USA), according to the manufacturer's instructions. Each experiment was repeated 3 times. Non-targeting small interfering RNA (siRNA) (5'-UUCUCCGAACGUGUCACGU-3') was used for the controls in the siRNA knock-down experiment.

Statistical Analysis

The Gaussian distribution for the quantitative proteomics data was fit and the SD was calculated. Differences of 2 times the SD between the sham + 32°C and sham + 37°C groups were set as thresholds for significantly differentially expressed proteins ($p < 0.05$) [36]. Other data are presented as the mean ± SD. SPSS 13.0 (IBM, Armonk, NY, USA) was used for analysis. Differences between groups were analyzed using one-way analysis of variance (ANOVA) followed by the Student–Newman–Keuls or Tukey's post-hoc analysis. All tests were 2-tailed and a p-value < 0.05 was considered to be statistically significant.

Results

TTM Overcomes TBI-Induced Necrosis of Neurons *in vitro*

To examine the effect of TTM on cell death in the presence of injury, we used an *in vitro* TBI model of mechanical stretch injury in human neuroblastoma-derived SH-SY5Y cells and mouse hippocampal HT-22 cells [17, 37]. The 6-h time point was selected to do the examination as there are reports

indicating that prior to 6 h necrosis is more important than apoptosis. Cells were either uninjured exposed to TTM (32°C) or normothermia (37°C) for 6 h, or were subjected to moderate (10.2 psi) stretch injury and harvested under either TTM or normothermia for 6 h post-injury. The effect of TTM was first assessed by phase-contrast microscopy (Fig. 1a) and real-time holographic imaging (Fig. 1b), which were used to characterize the cellular changes. In the presence of stretch injury, a significant reduction in cell area ($p < 0.01$) and cell volume ($p < 0.001$) was seen compared with that in the uninjured control group. After 6 h exposure to TTM (32°C), the cells became smaller (SH-SY5Y: from 279 to 183 μm^2) or larger (HT-22: from 176 to 277 μm^2) in surface area but greater (SH-SY5Y: from 467 to 571 μm^3; HT-22: from 1419 to 1720 μm^3) in volume compared with injured cells exposed to 37°C ($p < 0.001$; Fig. 1c).

We also examined the effect of TTM on neuronal cell death and viability, as assessed by PI positivity (Fig. 1d) and cell

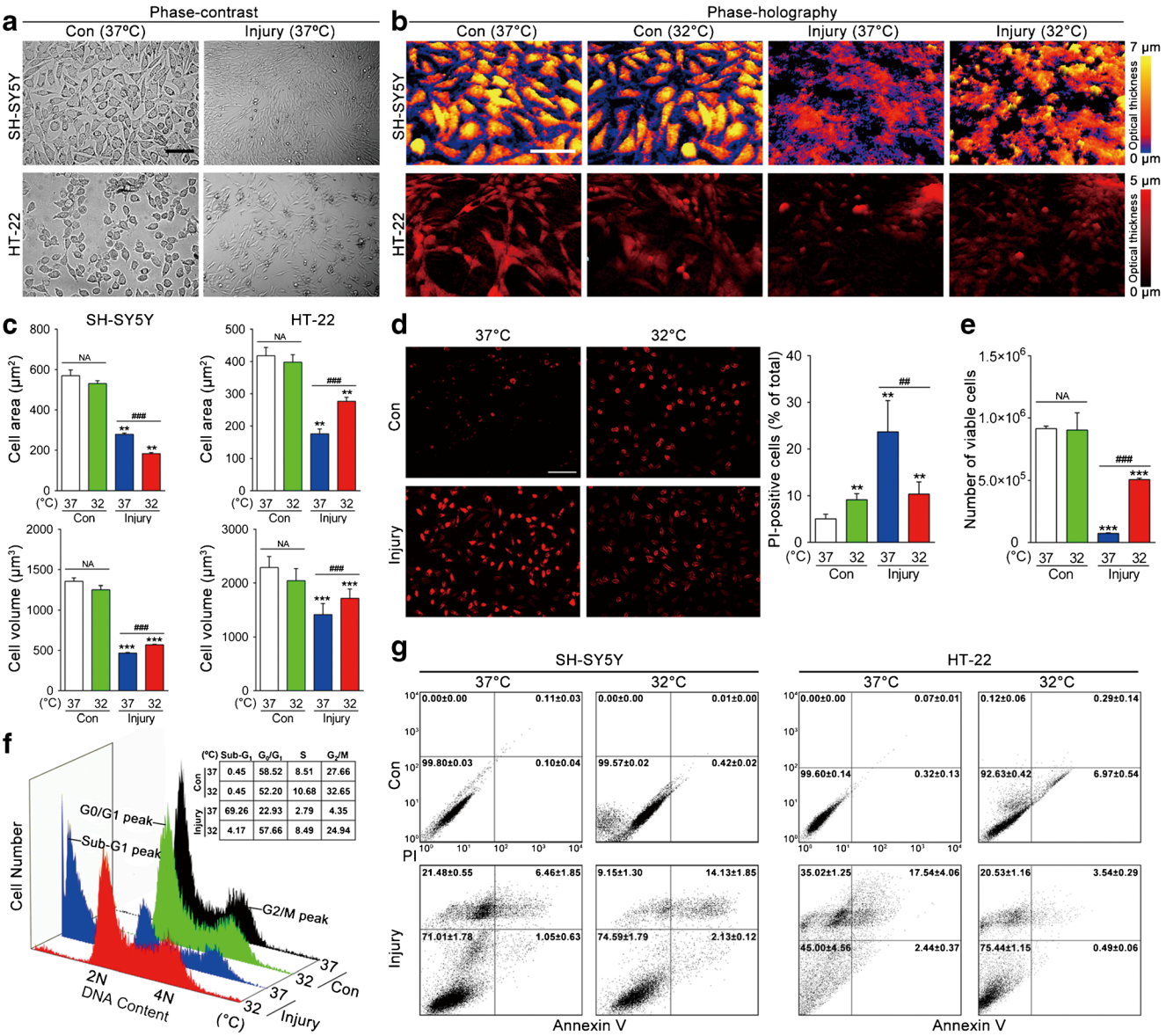

Fig. 1 Effects of targeted temperature management (TTM) on SH-SY5Y and HT-22 cells with traumatic brain injury-like damage. SH-SY5Y and HT-22 cells were either uninjured exposed to TTM (32°C) or normothermia (37°C), or subjected to stretch injury and harvested either 32°C or 37°C treatment for 6 h. The morphological changes were detected by (**a**) phase-contrast microscopy and (**b**) phase-holographic microscopy. (**c**) The mean cell area and volume were measured by digital holographic microscopy assay. (**d**) SH-SY5Y cell death was analyzed by propidium iodine (PI) labeling and counts were performed on PI-positive cells. (**e**) Quantification of SH-SY5Y cell viability was then measured using 0.4% trypan blue with the automated Countess system. (**f**) Representative flow cytometry analysis of SH-SY5Y cell-cycle distribution, expressed as the percentage of cells at sub-G_1, G_0/G_1, S, and G_2/M phase. (**g**) Necrosis and apoptosis were measured with Annexin V/PI labeling by flow cytometry. $^*p < 0.05$, $^{**}p < 0.01$, $^{***}p < 0.001$ *vs* uninjured control (37°C); $^{\#\#}p < 0.01$ and $^{\#\#\#}p < 0.001$ *vs* injured cells (37°C). Error bars represent SD ($n = 3$ independent experiments). NS indicates $p > 0.05$

counting (Fig. 1e) assays, respectively. Strikingly, stretch injury induced extensive SH-SY5Y cell death ($p < 0.01$) and resulted in a reduction in the number of viable cells ($p < 0.001$) compared with uninjured control cells, whereas the sensitivity of cells to stretch injury exposed to TTM was significantly lower than that of 37°C, as evidenced by PI positivity ($p < 0.01$) and cell viability ($p < 0.001$), as well as HT-22 cells (data not shown).

Cell-cycle phase distribution was then detected by flow cytometry to monitor the efficacy of TTM treatment. As demonstrated in Figure 1f, exposure to 37°C caused a significant accumulation of the injured SH-SY5Y cells in sub-G_1 phase (69.26%) compared with that of the uninjured cells (0.45%). However, TTM treatment considerably decreased sub-G_1 populations (from 69.26% to 4.17%). Further investigation into the TBI-induced cell death was performed through necrosis that occurs in the early phase, or apoptosis that occurs in the late phase after injury. Necrosis and apoptosis of SH-SY5Y and HT-22 cells postinjury were quantified using Annexin V/PI (Fig. 1g). To our surprise, stretch injury can induce necrosis in the early phase of SH-SY5Y cells as detected by PI, in which the percentage of necrotic cells increased significantly (from 0.00 ± 0.00% to 21.48 ± 0.55%). After TTM treatment, cells showed a sharp reduction in proportion of necrosis (9.15 ± 1.30%) compared with that of normothermia ($p < 0.05$; Fig. 1g, left). Similar results were obtained with HT-22 cells (Fig. 1g, right). Altogether, these *in vitro* results suggest that TTM overcomes TBI-induced damage of neurons.

TTM Decreases Neurological Damage and Attenuates Neurodegeneration Post-TBI *in vivo*

To gain further insight into the role of TTM and its cerebroprotective effect in TBI-induced damage, we used an *in vivo* TBI model of CCI injury. Animals were subjected to sham or CCI, followed by 6 h of TTM (32°C) or normothermia (37°C). Six rats in each group were randomly chosen for T2-weighted MRI analysis at 1 to 4 days post-CCI, and images from representative signal changes that occurred over time are shown in Figure 2(a). One to 4 days after CCI, rats exposed to 37°C displayed marked hyperintensities in the ipsilateral cortex and hippocampus due to vascular or cytotoxic edema, trauma-associated hydrocephalus, and extensive lesion spreading from the cortex to the hippocampus compared with sham animal. In contrast, TTM substantially reduced lesion size in injured rats, showing considerable sparing of large areas of brain tissue, notably the ipsilateral hippocampus. This was confirmed in fixed brain tissue sections (Fig. 2b) and then quantified in multiple coronal sections by cresyl violet staining (Fig. 2c). Quantitative analyses showed that lesion volume measured at 24 h after CCI exposed to 37°C was 38.7 ± 2.8 mm^3 *versus* only 1.5 ± 0.1 mm^3 for sham rats ($p < 0.01$). In contrast, TTM significantly reduced CCI-induced lesion volumes (11.2 ± 0.9 mm^3) compared with the CCI + 37°C group, which was declined by 71% ($p < 0.01$). Furthermore, we used FJC staining (Fig. 2d) to evaluate the potency of TTM in preventing neurodegeneration following TBI. FJC positivity was observed predominantly in the pericontusional area and the number of positive cells was sharply increased at 24 h post-CCI *versus* sham ($p < 0.01$). Differently, FJC-positive cells were significantly attenuated by TTM compared with the CCI + 37°C group ($p < 0.01$).

TTM Attenuates Cerebrovascular Histopathology and Improves Behavioral Outcome after TBI *in vivo*

The effect of TTM inhibition on TBI-induced cerebrovascular histopathology was evaluated by several techniques. First, rCBF in the cerebral cortex was continuously monitored (Fig. 3a). We found that no changes in rCBF were recorded in sham rats exposed to 37°C or 32°C (111.03 ± 9.78 *vs* 102.14 ± 7.77 ml/100 g/min; $p > 0.05$) at 24 h after CCI. On the other hand, CCI-injured exposed to 37°C showed a significant decrease of ipsilateral rCBF (36.76 ± 1.95 ml/100 g/min; $p < 0.01$). In contrast, the rCBF depression attenuated rapidly to 67.43 ± 7.39 ml/100 g/min ($p < 0.01$) in CCI-injured rats exposed to 32°C within the observation period. Next, quantification of brain water content was determined by examining the dry:wet ratio (Fig. 3b). CCI-induced rats exposed to 37°C developed significant brain edema in the traumatized hemisphere (83.56 ± 0.56%) 24 h after CCI compared with the sham group (77.21 ± 0.88%; $p < 0.001$), whereas brain water content in the contralateral hemisphere was similar in the different groups. Importantly, however, the increase in brain water content was significantly lower in the ipsilateral hemisphere of the CCI + 32°C rats (78.55 ± 0.87%; $p < 0.01$) compared with the CCI + 37°C group, indicating the low accumulation of water in the brain tissue. Finally, we examined EB dye extravasation in the restricted area around the contusion to evaluate the role of BBB in edema formation (Fig. 3c). At 24 h after injury, the extravasation was significantly higher in the CCI + 37°C group (274.46 ± 19.72 μg/g; $p < 0.001$) compared with sham control (108.65 ± 14.21 μg/g) in the ipsilateral hemisphere. However, the extravasation demonstrated lower values in the CCI + 32°C group (148.91 ± 18.99 μg/g) than these in the CCI + 37°C group ($p < 0.01$). Overall, these results suggest that TTM attenuates TBI-induced cerebrovascular histopathology, such as dysregulation of cerebrovascular blood flow, disruption of BBB, and cerebral edema formation.

To test whether TTM improved functional performance of rats after TBI, the mNSS and MWM tests were performed in the different groups. Significantly lower mNSS scores were found to be markedly improved in TTM animals compared with those in the normothermia groups on days 1, 2, and 3 after CCI (all $p < 0.01$; Fig. 3d). Furthermore, MWM was used

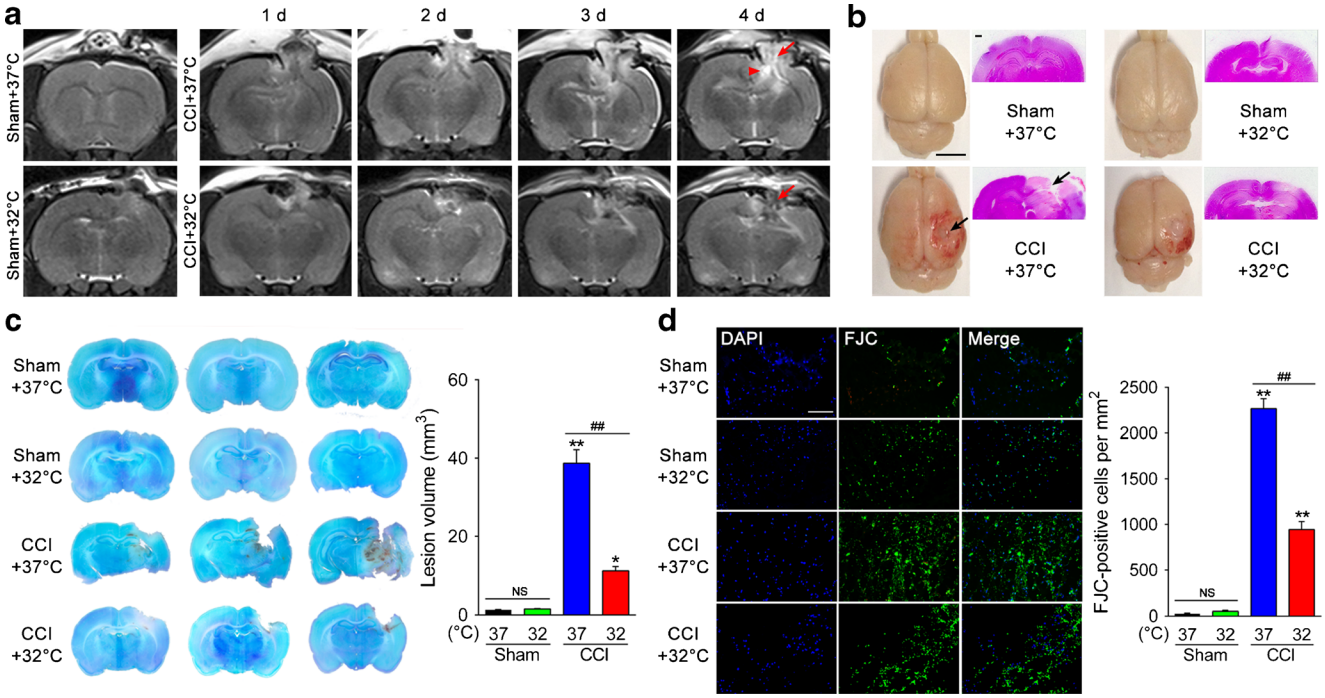

Fig. 2 Effects of targeted temperature management (TTM) on neurological damage and neurodegeneration after traumatic brain injury (TBI). (**a**) Representative T2-weighted magnetic resonance images at 1–4 days post-TBI. TTM reduces lesion size (arrow) and trauma-associated hydrocephalus (arrowhead) ($n = 6$/group). (**b**) Cortical contusion impact (CCI)-induced TBI created a focal lesion (arrow) in the right hemisphere of the rat brain (scale bar = 5 mm) at 24 h post-TBI. Representative images of hematoxylin and eosin-stained sections, highlighting considerable sparing of brain tissue in CCI + 32°C rats (scale bar = 500 μm). (**c**) At 24 h postinjury, brains were sectioned and stained with cresyl violet. Contralateral (left hemisphere) and ipsilateral (right hemisphere) substructure volumes were calculated in multiple sections per rat. Representative images from 3 consecutive sections per rat. Quantification of lesion volume was then assessed by subtracting the ipsilateral volume from the contralateral volume. (**d**) Assessment of neurodegeneration by Fluoro-Jade C (FJC) staining. Neurodegeneration observed in the pericontusional area 24 h after CCI was attenuated by TTM (scale bar = 40 μm). $^{*}p < 0.05$ and $^{**}p < 0.01$ *vs* sham + 37°C; $^{\#\#}p < 0.01$ *vs* CCI + 37°C. Error bars represent SD (n = 3/group). DAPI = 4',6-diamidino-2-phenylindole. NS indicates $p > 0.05$

to detect the spatial learning and memory for 7 consecutive days, starting on PID day 11 after TBI. Surprisingly, the CCI + 32°C group showed significantly shortened escape latencies ($p < 0.05$ or $p < 0.01$; Fig. 3e) from day 12 to day 17 post-CCI and increased time spent in the target quadrant ($p < 0.01$; Fig. 3f) relative to the CCI + 37°C group. Altogether, these *in vivo* results confirmed that behavioral outcome is negatively affected by TBI, such as neurological dysfunction or cognitive deficits, and can be improved by TTM.

Protein Identification, Quantification, and Bioinformatics Analysis of Candidate Molecules Associated with TTM Post-TBI

Although TTM has been long associated with TBI, its specific role in mediating damaging pathways and signaling cascades is not well understood. Using a newly developed quantitative proteomics by the 4-labeled iTRAQ protocol, we performed global profiling of protein expression from the brain tissue of rats, which were subjected to sham or CCI, followed by 6 h of TTM (32°C) or normothermia (37°C; Fig. 4a). The functions of the differentially expressed proteins were analyzed using DAVID, IPA, and Cytoscape version 3.3. GO annotation analysis was performed using DAVID and *R. norvegicus* was selected as the background and species. The significance was determined as recommended by the authors of DAVID, with slight modifications, according to the Benajmini correction of $p < 0.05$. The IPA software (version 14400082; Ingenuity Systems) was used for signaling pathway analysis of the altered proteins. The PPI network was generated using the CluePedia plugin of Cytoscape 3.2.1. For biological function analysis, the diagram was plotted based on the proteins with the highest score from both IPA and PPI analyses.

The results showed that the distribution of $\log_2$ (sham + 32°C/sham + 37°C) ratio could be fit to a Gaussian curve with a SD of 0.22 (n = 1526), that of $\log_2$ (CCI + 37°C/sham + 37°C) ratio with a SD of 0.28 (n = 1523), and 1529 proteins were quantified with a SD of 0.30 for the distribution of $\log_2$ (CCI + 32°C/sham + 37°C) ratio (Fig. 4b). In the sham + 32°C/sham + 37°C groups, 163 proteins were changed, with 127 proteins being upregulated and 36 proteins being downregulated. After TBI, 71 proteins were changed, with 42 proteins being upregulated and 29 proteins being downregulated. TTM changed 41 proteins after TBI, with 16 proteins being upregulated and 25 being downregulated. Interestingly, we noticed that the amount of altered proteins in the CCI +

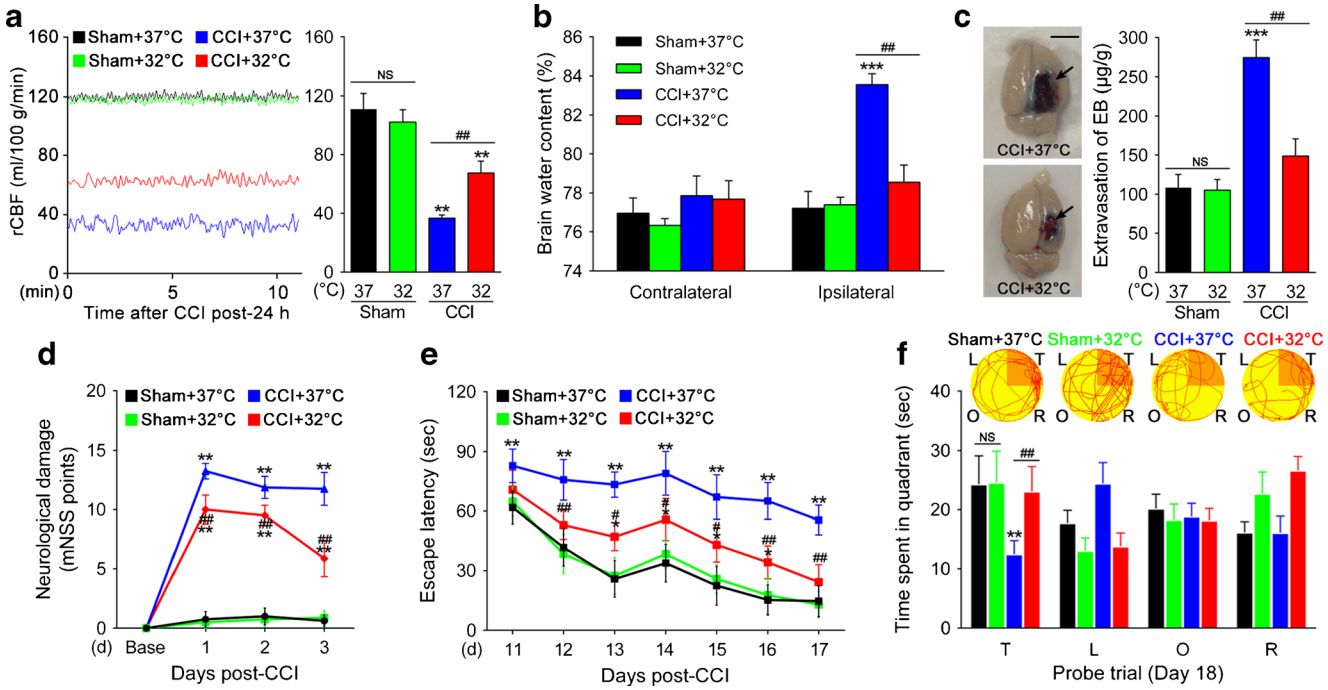

Fig. 3 Effects of targeted temperature management (TTM) on cerebrovascular histopathology and behavioral outcome post-traumatic brain injury (TBI). (**a**) TTM increases regional cerebral blood flow (rCBF) 24 h after TBI. Representative original recording of ipsilateral rCBF for 10 min. Values are expressed as mean ± SD (n = 6/group). (**b**) Graph showing increased brain water content (determined by dry:wet ratio) in the traumatized hemisphere 24 h post-TBI, whereas TTM decreases the accumulation of water in the tissue (n = 3/group). (**c**) Blood–brain barrier integrity was measured by assessing the extravasation of Evans blue (EB) dye. The extravasation of EB dye in brain samples from cortical contusion impact (CCI) + 37°C or 32°C rats is shown. (**d**) Modified neurological severity (mNSS) score was assigned 1, 2, and 3 days post-TBI (n = 20/group). (**e**) The Morris water maze test was used to detect the spatial learning and memory for 7 consecutive days, starting on post-injury day (PID) 11 after TBI (n = 20/group). TTM significantly shortened escape latency during PID 12–17. (**f**) Representative path tracings in each quadrant during the probe trial on PID 18 (T = target quadrant; R = right quadrant; O = opposite quadrant; L = left quadrant). $^{**}p < 0.01$ and $^{***}p < 0.001$ *vs* sham (37°C); $^{\#}p < 0.05$ and $^{\#\#}p < 0.01$ *vs* CCI (37°C). Error bars represent SD. NS indicates $p > 0.05$

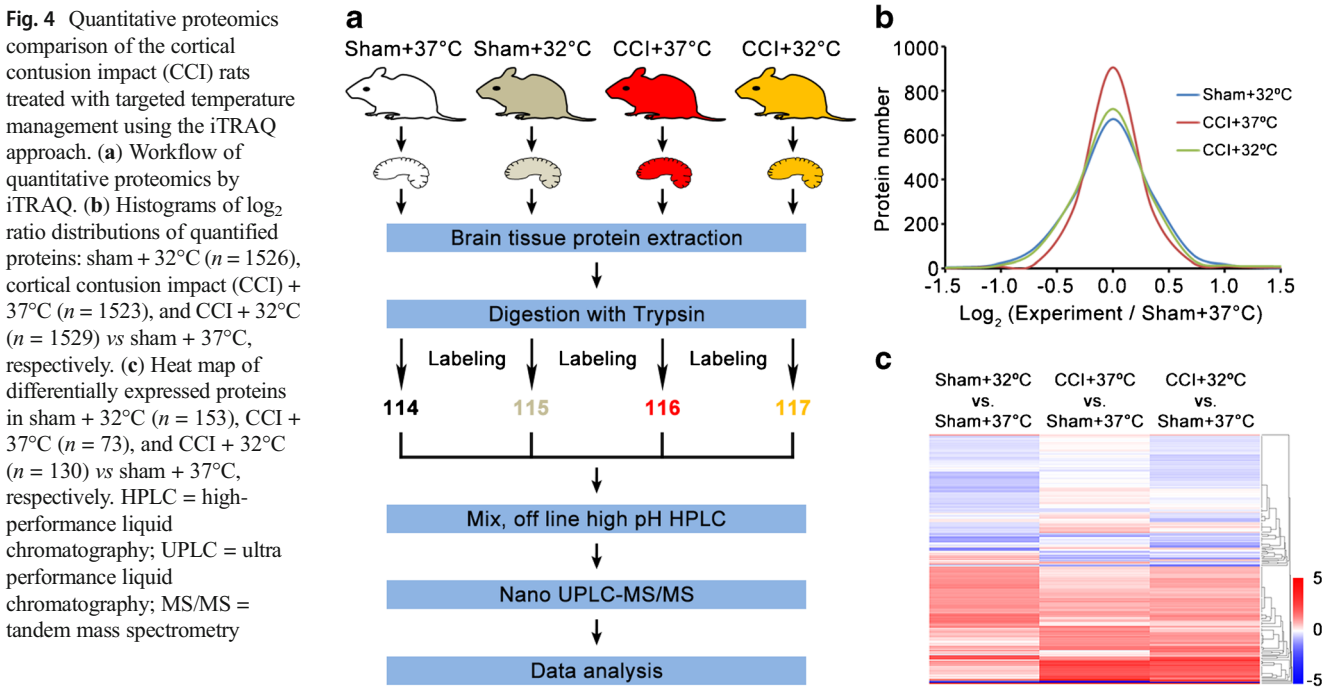

Fig. 4 Quantitative proteomics comparison of the cortical contusion impact (CCI) rats treated with targeted temperature management using the iTRAQ approach. (**a**) Workflow of quantitative proteomics by iTRAQ. (**b**) Histograms of $\log_2$ ratio distributions of quantified proteins: sham + 32°C (n = 1526), cortical contusion impact (CCI) + 37°C (n = 1523), and CCI + 32°C (n = 1529) *vs* sham + 37°C, respectively. (**c**) Heat map of differentially expressed proteins in sham + 32°C (n = 153), CCI + 37°C (n = 73), and CCI + 32°C (n = 130) *vs* sham + 37°C, respectively. HPLC = high-performance liquid chromatography; UPLC = ultra performance liquid chromatography; MS/MS = tandem mass spectrometry

32°C group was larger than that in the CCI + 37°C group. The results of cluster analysis for differentially expressed proteins showed that CCI + 32°C treatment could significantly reverse many protein expression trends compared with the CCI + 37°C group (Fig. 4c). The quantification of differentially expressed proteins is shown in Table S1.

Subsequently, GO analysis for the altered proteins was submitted to a DAVID analysis, which included biological process and cellular component analysis. The results showed that blood coagulation, response to wounding, and hemostasis processes were enriched in the extracellular space, platelet alpha granule lumen, vesicle lumen, and secretory granule in the CCI + 37°C group *versus* the sham + 37 °C group (Fig. 5a). GO analysis of the CCI + 32°C *versus* CCI + 37°C groups showed that macromolecular complex assembly, response to mercury ion processes and cytoplasmic membrane-bounded vesicle, cytosol, and pigment granule components were enriched (Fig. 5b). We also noticed that the related molecule expression levels, such as Akt, discs large homolog 1 (DLG1), and membrane-associated guanylate kinase inverted 2 (MAGI2), of the nervous system development network in the CCI + 37°C group were significantly downregulated (Fig. 5c). The TTM treatment might regulate the related molecules expression levels of cellular function and maintenance function, including Akt, SEC14L2, DSP, and TCP1, and these proteins could be involved in the neuroprotective function (Fig. 5d).

To explore the global possible PPIs using the Cytoscape, we found that the fibrinogen gamma chain (FGG), fibrinogen alpha chain (FGA), fibrinogen beta chain (FGB), apolipoprotein A1 (APOA1), glutathione S-transferase P (GSTP1), serphin family C member 1 (SERPINC1), plasminogen (PLG), apolipoprotein H (APOH), and histidine-rich glycoprotein (HRG) were responsible for hemostasis, platelet aggregation, blood coagulation, and many other processes in the CCI + 37°C group (Fig. 5e). Meanwhile, TTM could alleviate the TBI-induced neurotrauma through regulation of hemostasis, platelet aggregation, blood coagulation, and many other processes (Fig. 5f).

Confirmation of iTRAQ Data in Rat Brain Tissue and Human CSF Post-TBI

Owing to the limitations of the rat database, the number of proteins validated in the quantitative proteomics analysis was limited, and not every differentially expressed protein could be classified when analyzed with DAVID, IPA, and Cytoscape. Moreover, in order to screen for the potential diagnostic biomarkers of TBI severity, this study focused on secretory proteins. In the purpose of hunting for proper potential biomarkers, the top-20 proteins for each upregulated and downregulated side after TBI intervention or after reversion of TBI effect with TTM were analyzed, and 11 molecules were sorted out to be the shared proteins. For screening biomarkers, this study selected upregulated secretory proteins after TBI intervention (downregulated proteins could be undetectable by ELISA). The results of the GO and IPA analyses for MS data showed that the expression levels of coagulation system-related molecules in the TTM groups, PLG, AT III, albumin, and FGG, were significantly decreased compared with those of the TBI groups ($p < 0.05$), indicating that TTM treatment can be an effective strategy applied for patients with TBI [38]. Considering that albumin, the most abundant protein in serum, could be influenced by liver function, infection, nutrition, and a number of other factors, it was excluded from the list for validation. Thus, 4 proteins were rendered for validation: PLG, ATI II, FGG, and TTR.

Meanwhile, the expression level of TTR in the TBI groups was significantly increased compared with that of the control group, and that of TTM groups was significantly decreased compared with that of the TBI group (Tables S2 and S3). A recent study showed that the accumulation or mutation of TTR, which is a potent scavenger of amyloid peptides in the central nervous system, would result in different organization of amyloidosis and neuronal degeneration [39]. Hence, we verified whether TTM was associated with significant change in the expression of a variety of factors involved in TBI among PLG, AT III, Fgg, and TTR *in vivo* using immunofluorescence.

The next step was to confirm the PLG, AT III, Fgg, and TTR findings in human samples. To do so, we used ventricular CSF from 20 patients with standard therapy or TTM + standard therapy at separate time points after injury (GCS from 3 to 15). The quantitative immunoblotting results showed that all patients' (7 with mild TBI: GCS 13–15 but with imaging revealing extradural and/or subdural hemorrhage, with mild bone fracture; 5 with moderate TBI: GCS 9–12; 8 with severe TBI: GCS 3–8 among whom 4 patients were subjected to standard therapy group and the other 4 to TTM+ standard therapy group) CSF at 1 day after trauma (acquired from 4 patients with severe TBI [GCS 3–8], 5 moderate TBI [GCS 9–12], and 7 mild TBI [GCS 13–15]) contained PLG, AT III, Fgg, and TTR but that the levels varied a lot. Furthermore, samples from patients with severe or moderate TBI (GCS 3–12) had markedly more of the proteins mentioned above than those from patients with mild TBI (GCS 13–15) at 1 day postinjury (Fig. 6a, left). We further examined the expression of PLG, AT III, Fgg, and TTR in the CSF samples at 1 and 3 days from 4 patients with severe TBI followed by standard therapy (37°C) and from 4 patients with severe TBI followed by TTM + standard therapy (32°C). The results suggest that samples of severe TBI + 37°C group showed increased levels of PLG, AT III, Fgg, and TTR over time, whereas the severe TBI + 32°C group had rather lower levels at 3 days after trauma compared with the levels at 1 day post-TBI (Fig. 6a, right).

Next, we addressed whether there were altered levels by using quantitative ELISA on patient CSF. The temporal profiles of CSF PLG, AT III, FGG, and TTR acquired from

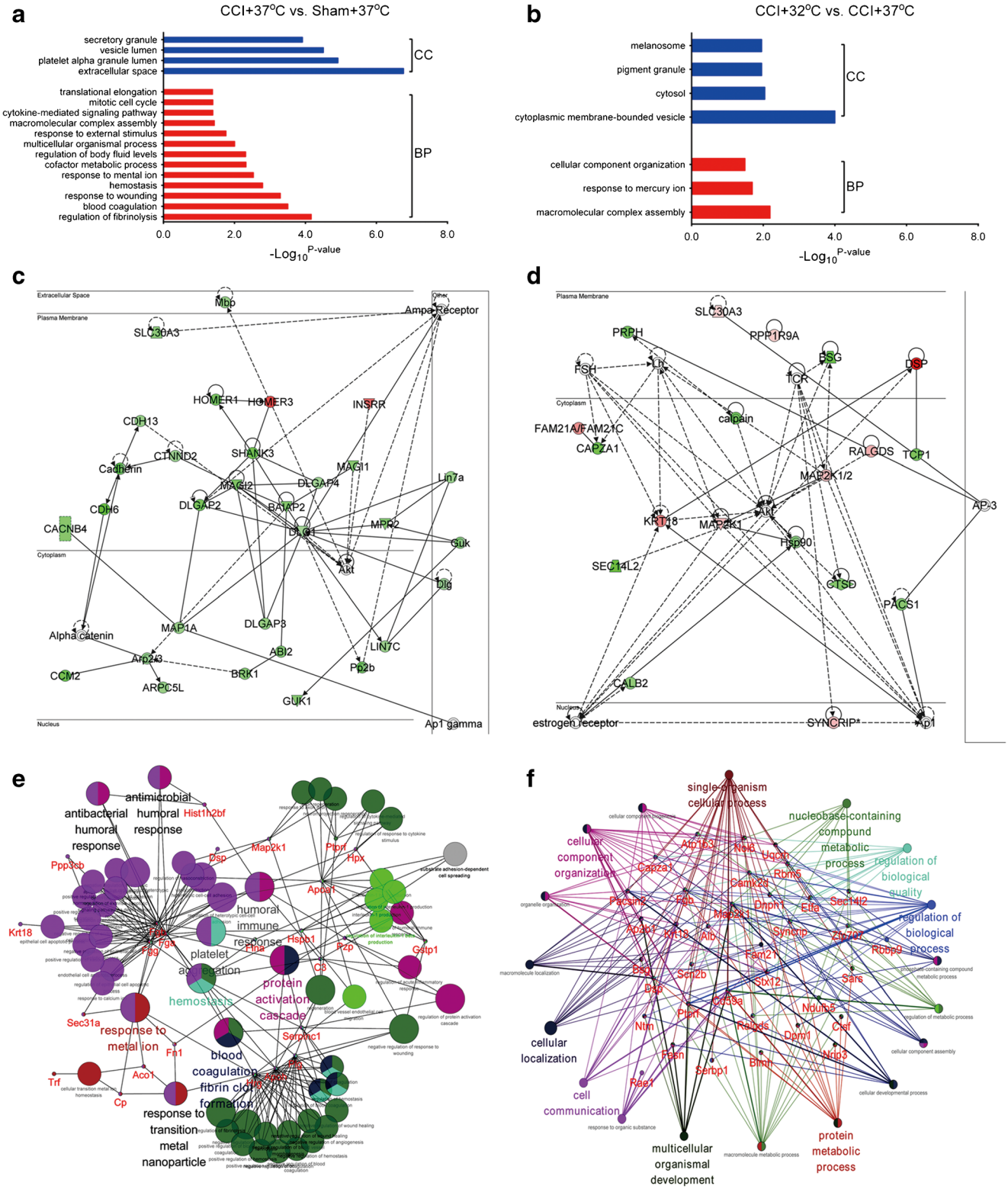

Fig. 5 Bioinformatics analysis for the differentially expressed proteins in the cortical contusion impact (CCI) rats treated with targeted temperature management. Diagram showing the biological process (BP) and cellular component (CC) of differentially expressed proteins of (**a**) CCI + 37°C *vs* sham + 37°C and (**b**) CCI + 32°C *vs* CCI + 37°C using DAVID analysis. Network of (**c**) CCI + 37°C *vs* sham + 37°C and (**d**) CCI + 32°C *vs* CCI + 37°C clustered by Ingenuity Pathway Analysis. Protein–protein interaction was generated by Cytoscape between (**e**) CCI + 37°C *vs* sham + 37°C and (**f**) CCI + 32°C *vs* CCI + 37°C

patients with severe TBI ($n = 4$, GCS 3–8), moderate TBI ($n = 5$, GCS 9–12), and mild TBI ($n = 7$, GCS 13–15) at 1 day after trauma are shown in Figure 6(b). The mean CSF PLG levels in patients with severe and moderate TBI (1336.83 ± 558.08 and 1456.38 ± 808.25 ng/ml) were sharply increased compared with that in patients with mild TBI (176.96 ± 182.55 ng/ml; $p = 0.0014$ and $p = 0.0042$, respectively). Additionally, as with PLG, the mean AT III, FGG, and TTR levels in patients with severe and moderate TBI were higher than those in patients with mild TBI [AT III: 127.81 ± 69.28 and 60.97 ± 37.95 *vs* 16.23 ± 10.99 ng/ml ($p = 0.0044$ and $p = 0.0225$); FGG: 78.49 ± 57.44 and 44.82 ± 6.37 *vs* 15.49 ± 7.30 ng/ml ($p = 0.0293$ and $p < 0.0001$); TTR: 4.52 ± 2.70 and 4.62 ± 2.22 *vs* 1.24 ± 1.39 ng/ml ($p = 0.0396$ and $p = 0.0147$)].

In addition, the temporal profiles of CSF proteins mentioned above acquired from patients with severe TBI with standard therapy or TTM therapy at separate time points after injury are shown in Figure 6(c). The results suggest that CSF PLG, AT III, and FGG did not change over time when examined 1 and 3 days after severe TBI with normothermia therapy ($p > 0.05$), but the mean TTR levels were significantly increased over time (4.52 ± 2.70 *vs* 19.29 ± 7.59 ng/ml; $p = 0.0191$). Additionally, the mean CSF PLG, AT III, and FGG levels were sharply lower in patients with TTM therapy at 3 days *versus* 1 day post-TBI [PLG: 1189.04 ± 497.11 *vs* 606.31 ± 109.00 ng/ml ($p = 0.0127$); AT III: 117.02 ± 3.43 *vs* 54.60 ± 18.03 ng/ml ($p = 0.0011$); FGG: 78.96 ± 10.91 *vs* 51.94 ± 7.19 ng/ml ($p = 0.0038$)], but CSF TTR did not change over time ($p > 0.05$). The results of Western blot and ELISA for these proteins were consistent with the proteomic data. Taken together, these data suggested that PLG, AT III, FGG, and TTR were present in human CSF after TBI, and TTM treatment showed the inverse change in expression pattern, supporting the notion that these molecules may be useful as future biomarkers associated with TTM. Nevertheless, these results should be taken with caution because the exact source of the CSF (EVD *vs* LP) could affect the results. Additional studies are necessary to examine this point.

siRNA and Cell Viability

In order to further explore the mechanisms of the identified proteins, the TTR, PLG, ATIII, and FGG genes were knocked down in HT-22 cells, and the 3-(4,5-dimethylthiazol-2-yl)-2,5-diphenyl tetrazolium assay was used to assess cell viability. The results showed that after TTR knockdown, the cell viability did not change significantly. However, the knockdown of PLG and AT III increased cell viability, whereas the FGG siRNA had a marginal effect, suggesting that the knockdown PLG and AT III (and FGG, to a lesser extent) can improve the recovery of CCI-induced injured cells. Nevertheless, the viability of the cells with gene knockdown was still significantly lower than those with TTM treatment (Fig. 7a). We can speculate that these three genes only

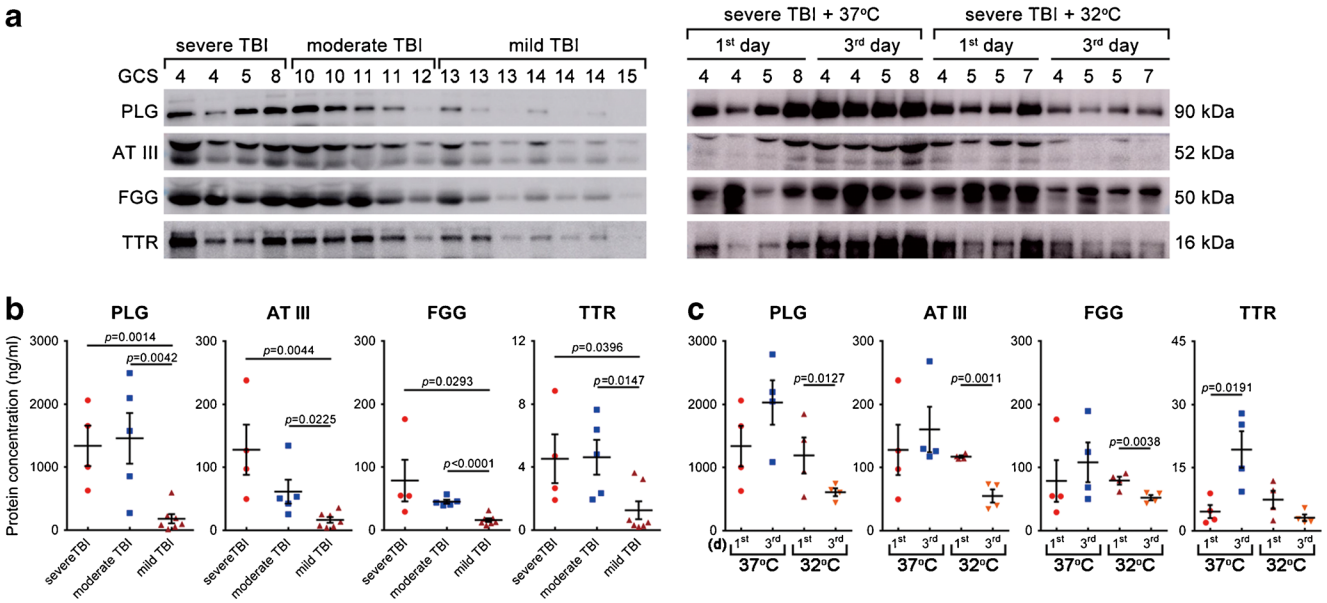

Fig. 6 Plasminogen (PLG), antithrombin III (AT III), fibrinogen gamma chain (FGG), and transthyretin (TTR) levels reflected injury magnitude, and the effect of TTM post-traumatic brain injury (TBI). (**a**) The levels of PLG, AT III, FGG, and TTR in 28 cerebrospinal fluid (CSF) samples were evaluated by Western blot, including 4 patients with severe TBI (Glasgow Coma Scale [GCS] 3–8), 5 with moderate TBI (GCS 9–12), 7 with mild TBI (GCS 13–15) with standard therapy at 1 day after trauma (left panel), and 4 patients with severe TBI (the same patients with that in the left panel) followed by standard therapy (37°C) and 4 with severe TBI followed by TTM + standard therapy (32°C) at 1 and 3 days postinjury (right panel). (**b**) Temporal profile of CSF PLG, AT III, FGG, and TTR levels (ng/ml) among patients with severe ($n = 4$), moderate ($n = 5$), and mild TBI ($n = 7$) with standard therapy at 1 day after trauma, and (**c**) in patients with severe TBI receiving standard therapy and TTM + standard therapy at 1 and 3 days postinjury were measured by enzyme-linked immunosorbent assay. Error bars represent SD

represent a part of the protective mechanisms of TTM, and the effects of TTM in improving cell injury repair might be achieved through other pathways in addition to the changes of the expression levels of PLG, AT III, and FGG.

Further investigation on the expression levels of FGG, AT III, and PLG (Fig. 7b, c, d) showed that the levels of these proteins were increased after cell damage, whereas TTM could reduce the expression of FGG, AT III, and PLG in damaged cells, but the application of TTM did not significantly change the levels of FGG, AT III, and PLG in undamaged cells, and the effect of FGG was more marginal than that of PLG and AT III. These findings suggest that the changes of FGG, AT III, and PLG by TTM occurred after cell damage. For AT III and PLG, TTM and gene knockdown showed synergistic effects. TTM further reduced the protein expression after knockdown. These findings suggest that the combined use of TTM in addition to ATIII and PLG knockdown could more effectively improve cell repair. In contrast, TTM increased FGG protein levels in the FGG gene knockdown group of damaged cells. We measured proliferating cell nuclear antigen (PCNA) and found that PCNA was decreased significantly after cell damage, whereas TTM treatment decreased the levels of PCNA (Fig. 7d). We speculated that TTM could not increase the proliferation of the cells.

Discussion

Previous *in vivo* and *in vitro* experimental studies showed the beneficial effects of TTM in TBI in fluid percussion injury (FPI) animal and scratch injury cell models [40–42]. In our previous studies, we found that post-traumatic TTM significantly improved survival of neurons and reduced β-amyloid and other indicators of abnormal protein accumulation [21]. Nevertheless, the pathology of TBI is so diverse that precise mechanisms underlying this phenomenon are still unclear, mainly because the phenotypic effects of TTM emerge through a currently intractable, not well-understood, multicellular process involving hundreds of interacting molecular components [13].

In the current study, we exposed neuron-like SH-SY5Y cells and mouse hippocampal HT-22 cells to 32°C following CIC, which is widely used as a cell model to investigate TBI *in vitro* [17, 43], and observed the accumulation of injured cells in sub-G_1 phase, PI-positive cells, and cell death, whereas TTM decreased sub-G_1 populations and the sensitivity of cells to stretch injury as evidenced by PI positivity and cell viability compared with normothermia, suggesting that TTM inhibition overcomes TBI-induced damage of neurons. Similar to our previous studies and other reports, TBI produces behavioral abnormalities and neurodegenerative changes resulting from regional patterns of cell death and circuit dysfunction [21, 44]. As supported by previous studies of

Fig. 7 Validation of the influence of plasminogen (PLG), antithrombin III (AT III), fibrinogen gamma chain (FGG), and transthyretin (TTR) on HT-22 cell viability by small interfering RNA (siRNA) treatment. (**a**) PLG, AT III, FGG, and TTR were knocked down in cells. Then targeted temperature management (TTM) was applied and CellTiter 96 AQueous One solution Cell Proliferation Assay was used to measure cell viability. (**b**) Effects of FGG knockdown and TTM on the expression of FGG and proliferating cell nuclear antigen (PCNA). (**c**) Effects of AT III knockdown and TTM on the expression of AT III and PCNA. (**d**) Effects of PLG knock down and TTM on the expression of PLG and PCNA. $^{*}p < 0.05$ *vs* the control group; $^{\#}p < 0.05$ *vs* the traumatic brain injury (TBI) group; $^{\&}p < 0.05$ *vs* the TBI + siRNA knockdown group. CIC = cell injury controller

TTM on TBI, we also demonstrated that using CCI rats as an *in vivo* model that TTM attenuated several phenotypes of animal post-TBI, markedly reduced cell death [7, 8, 11], BBB leakage [45–47], cortical lesion volume [48], cerebrovascular histopathology [49, 50], and improved behavioral and pathological outcomes [51]. These results may help determine both the safety and efficacy for postinjury TTM, and such laboratory models (*in vitro* or *in vivo*) may present an ideal opportunity for the application of proteomic technological approach to biomarker discovery after TBI.

Systems biology is a crucial approach to investigate the complex, multifactorial nature of secondary cellular interactions to TBI, from which a testable hypothesis about the underlying TBI-related molecular mechanisms that can be experimentally validated is generated by the analysis of data-driven, high-throughput genomics or proteomics data sets of biomolecules and their interactions rather than traditional research approaches [52–54]. In the present study we applied isobaric peptide tags (iTRAQ) and multidimensional LC-MS/MS to identify proteins that were differentially expressed in 32°C *versus* 37°C injured brain specimens derived from a CCI model of TBI. Of the altered proteins after TBI, regulation of fibrinolysis and blood coagulation, which were the most important processes, were reported in terms of vascular injury and hemorrhage [55]. Besides, another important process—response to wounding—is another natural response to injury, as shown by altered mitotic cell cycle, such as revealed by neural stem cell proliferation after TBI. Response to metal ions correspond to Ca^{2+} stimuli, and cytokine-mediated signaling pathways correspond to the tumor necrosis factor-α and interleukin-1β stimuli. TTM seems to reduce these dysfunctions. Above all, the present study is only the first systematic study of TBI and TTM, and additional studies are still needed to confirm the TTM effects comprehensively.

TBI is a complicated process because of various injury causes, locations, and severities. Biomarkers for function outcome and prognosis are urgently needed. In the past decades, a few biomarkers have been identified. For example, S100B is a widely used protein for the assessment and prediction of TBI [18, 56–58]. Recently, MIF was found to change along with inflammation factors and could be a prognosis biomarker for

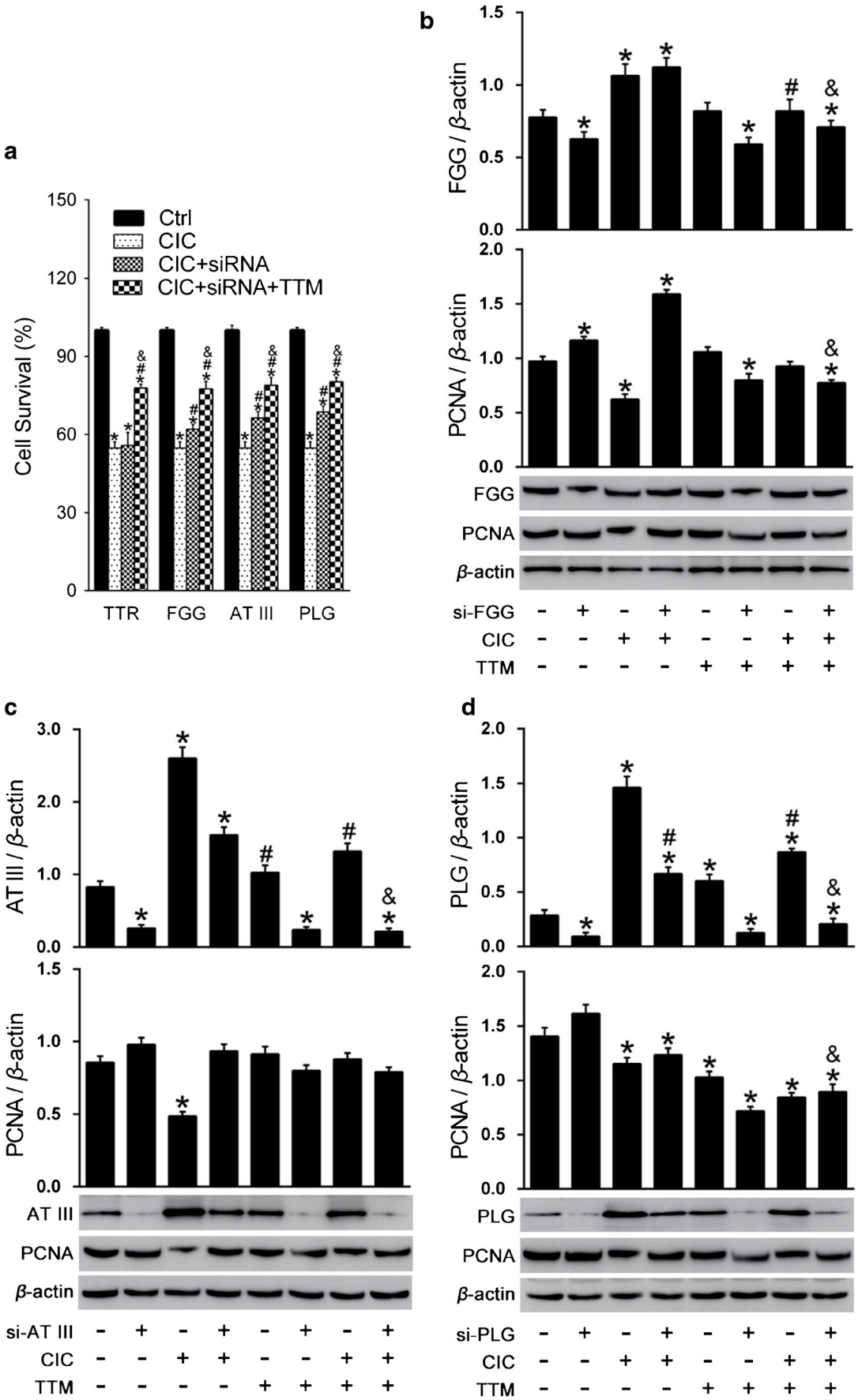
a
Cell Survival (%)
150
120
90
60
30
0
Ctrl
CIC
CIC+siRNA
CIC+siRNA+TTM
TTR
FGG
AT III
PLG
b
FGG / β-actin
PCNA / β-actin
FGG
PCNA
β-actin
si-FGG
CIC
TTM
c
AT III / β-actin
PCNA / β-actin
AT III
PCNA
β-actin
si-AT III
CIC
TTM
d
PLG / β-actin
PCNA / β-actin
PLG
PCNA
β-actin
si-PLG
CIC
TTM

good clinical outcome [59]. Sharma et al. [60] tested 87 potential serum biomarkers from 110 patients with mild TBI, and found a biomarker panel that identifies complicated mild TBI from uncomplicated mild TBI. Another systematic biomarker screening study—also based on antibody-based proteomics—was conducted on normoxic or hypoxic TBI models, and potential biomarkers for TBI were identified but failed to separate normoxic or hypoxic TBI models [58].

In the present study, we also focused on screening a series of altering expression molecules in CCI with TTM treatment, including Fgg, fibrinogen alpha chain, fibrinogen beta chain, apolipoprotein A1, glutathione S-transferase P, serphin family C member 1, PLG, apolipoprotein H, and histidine-rich glycoprotein, which are involved in vital biological processes, such as hemostasis, platelet aggregation, and blood coagulation. In particular, PLG, AT III, Fgg, and TTR could be used as assessment criteria of TBI healing after TTM treatment, and the expression pattern was confirmed by immunostaining on tissue from CCI rats treated with TTM, as well as by Western blot and ELISA assay on CSF samples acquired from patients with TBI followed by TTM.

In conclusion, based on iTRAQ quantitative proteomics profiling, we have generated an extensive and unique data set of protein expression profiles that recapitulates the change of proteins in TBI treated with TTM. The validation of the iTRAQ result for the PLG, AT III, FGG, and TTR proteins suggests that the combined proteomics and bioinformatics analysis applied has generated valid candidates that may be used for diagnostic and prognostic counseling of patients with TBI. These results may provide more accurate information about TBI status and clinical outcome, and may be further evaluated for their role associated with TTM in the progression from TBI.

Acknowledgments This work was supported by grants from the National Natural Science Foundation of China (31200809), Science & Technology Program of Tianjin, China (15ZXLCSY00040), and Technology Research Projects (AWS15J001).

Required Author Forms Disclosure forms provided by the authors are available with the online version of this article.

References

1. Manley GT, Maas AI. Traumatic brain injury: an international knowledge-based approach. JAMA 2013;310:473-474.
2. Jiang JY. Head trauma in China. Injury 2013;44:1453-1457.
3. Corrigan JD, Selassie AW, Orman JA. The epidemiology of traumatic brain injury. J Head Trauma Rehabil 2010;25:72-80.
4. Nunnally ME, Jaeschke R, Bellingan GJ *et al.* Targeted temperature management in critical care: a report and recommendations from five professional societies. Crit Care Med 2011;39:1113-1125.
5. Zhao CC, Wang CF, Li WP *et al.* Mild hypothermia promotes pericontusion neuronal sprouting via suppressing suppressor of cytokine signaling 3 expression after moderate traumatic brain injury. J Neurotrauma 2017;34:1636-1644.
6. Truettner JS, Bramlett HM, Dietrich WD. Posttraumatic therapeutic hypothermia alters microglial and macrophage polarization toward a beneficial phenotype. J Cereb Blood Flow Metab 2016;271678X16680003.
7. Zhang HB, Cheng SX, Tu Y, Zhang S, Hou SK, Yang Z. Protective effect of mild-induced hypothermia against moderate traumatic brain injury in rats involved in necroptotic and apoptotic pathways. Brain Inj 2017;31:406-415.
8. Liu T, Zhao DX, Cui H *et al.* Therapeutic hypothermia attenuates tissue damage and cytokine expression after traumatic brain injury by inhibiting necroptosis in the rat. Sci Rep 2016;6:24547.
9. Diller KR, Zhu L. Hypothermia therapy for brain injury. Annu Rev Biomed Eng 2009;11:135-162.
10. Gibbons H, Sato TA, Dragunow M. Hypothermia suppresses inducible nitric oxide synthase and stimulates cyclooxygenase-2 in lipopolysaccharide stimulated BV-2 cells. Brain Res Mol Brain Res 2003;110:63-75.
11. Amin FU, Shah SA, Kim MO. Vanillic acid attenuates Abeta1-42-induced oxidative stress and cognitive impairment in mice. Sci Rep 2017;7:40753.
12. Urbano LA, Oddo M. Therapeutic hypothermia for traumatic brain injury. Curr Neurol Neurosci Rep 2012;12:580-591.
13. Andriessen TM, Jacobs B, Vos PE. Clinical characteristics and pathophysiological mechanisms of focal and diffuse traumatic brain injury. J Cell Mol Med 2010;14:2381-2392.
14. Clifton GL, Valadka A, Zygun D *et al.* Very early hypothermia induction in patients with severe brain injury (the National Acute Brain Injury Study: Hypothermia II): a randomised trial. Lancet Neurol 2011;10:131-139.
15. Ottens AK, Bustamante L, Golden EC *et al.* Neuroproteomics: a biochemical means to discriminate the extent and modality of brain injury. J Neurotrauma 2010;27:1837-1852.
16. Chahrour O, Cobice D, Malone J. Stable isotope labelling methods in mass spectrometry-based quantitative proteomics. J Pharm Biomed Anal 2015;113:2-20.
17. Morrison B, 3rd, Elkin BS, Dolle JP, Yarmush ML. In vitro models of traumatic brain injury. Annu Rev Biomed Eng 2011;13:91-126.
18. Thelin EP, Nelson DW, Bellander BM. A review of the clinical utility of serum S100B protein levels in the assessment of traumatic brain injury. Acta Neurochir (Wien) 2017;159:209-225.
19. Fujita M, Oda Y, Yamashita S et al. Early-stage hyperoxia is associated with favorable neurological outcomes and survival after severe traumatic brain injury: a post-hoc analysis of the brain hypothermia study. J Neurotrauma 2017;19
20. Andrews PJ, Sinclair HL, Rodriguez A et al. Hypothermia for intracranial hypertension after traumatic brain injury. N Engl J Med 2015;373:2403-2412.
21. Cheng SX, Zhang S, Sun HT, Tu Y. Effects of mild hypothermia treatment on rat hippocampal beta-amyloid expression following traumatic brain injury. Ther Hypothermia Temp Manag 2013;3:132-139.
22. Loov C, Nadadhur AG, Hillered L, Clausen F, Erlandsson A. Extracellular ezrin: a novel biomarker for traumatic brain injury. J Neurotrauma 2015;32:244-251.
23. Silasi G, Colbourne F. Unilateral brain hypothermia as a method to examine efficacy and mechanisms of neuroprotection against global ischemia. Ther Hypothermia Temp Manag 2011;1:87-94.
24. Jin Y, Lei J, Lin Y, Gao GY, Jiang JY. Autophagy inhibitor 3-MA weakens neuroprotective effects of posttraumatic brain injury moderate hypothermia. World Neurosurg 2016;88:433-446.
25. Marion DW, Penrod LE, Kelsey SF et al. Treatment of traumatic brain injury with moderate hypothermia. N Engl J Med 1997;336:540-546.

26. Hsieh CL, Niemi EC, Wang SH et al. CCR2 deficiency impairs macrophage infiltration and improves cognitive function after traumatic brain injury. J Neurotrauma 2014;31:1677-1688.
27. Bareyre F, Wahl F, McIntosh TK, Stutzmann JM. Time course of cerebral edema after traumatic brain injury in rats: effects of riluzole and mannitol. J Neurotrauma 1997;14:839-849.
28. Zhao J, Pati S, Redell JB, Zhang M, Moore AN, Dash PK. Caffeic acid phenethyl ester protects blood-brain barrier integrity and reduces contusion volume in rodent models of traumatic brain injury. J Neurotrauma 2012;29:1209-1218.
29. Anderson KJ, Fugaccia I, Scheff SW. Fluoro-jade B stains quiescent and reactive astrocytes in the rodent spinal cord. J Neurotrauma 2003;20:1223-1231.
30. Gold EM, Su D, Lopez-Velazquez L et al. Functional assessment of long-term deficits in rodent models of traumatic brain injury. Regen Med 2013;8:483-516.
31. Tu Y, Chen C, Sun HT et al. Combination of temperature-sensitive stem cells and mild hypothermia: a new potential therapy for severe traumatic brain injury. J Neurotrauma 2012;29:2393-2403.
32. Zhai L, Chang C, Li N et al. Systematic research on the pretreatment of peptides for quantitative proteomics using a C(1)(8) microcolumn. Proteomics 2013;13:2229-2237.
33. Huang da W, Sherman BT, Lempicki RA. Systematic and integrative analysis of large gene lists using DAVID bioinformatics resources. Nat Protoc 2009;4:44-57.
34. Huang da W, Sherman BT, Lempicki RA. Bioinformatics enrichment tools: paths toward the comprehensive functional analysis of large gene lists. Nucleic Acids Res 2009;37:1-13.
35. Lei J, Gao G, Mao Q et al. Rationale, methodology, and implementation of a nationwide multicenter randomized controlled trial of long-term mild hypothermia for severe traumatic brain injury (the LTH-1 trial). Contemp Clin Trials 2015;40:9-14.
36. Jin X, Xu Z, Cao J, et al. Proteomics analysis of human placenta reveals glutathione metabolism dysfunction as the underlying pathogenesis for preeclampsia. BBA 2017;1865:1207-1214.
37. Jin G, Liu B, You Z, et al. Development of a novel neuroprotective strategy: combined treatment with hypothermia and valproic acid improves survival in hypoxic hippocampal cells. Surgery 2014;156:221-228.
38. de Oliveira Manoel AL, Neto AC, Veigas PV, Rizoli S. Traumatic brain injury associated coagulopathy. Neurocrit Care 2015;22:34-44.
39. Benoit CE, Rowe WB, Menard C, Sarret P, Quirion R. Genomic and proteomic strategies to identify novel targets potentially involved in learning and memory. Trends Pharmacol Sci 2011;32:43-52.
40. Bregy A, Nixon R, Lotocki G et al. Posttraumatic hypothermia increases doublecortin expressing neurons in the dentate gyrus after traumatic brain injury in the rat. Exp Neurol 2012;233:821-828.
41. Huang T, Solano J, He D, Loutfi M, Dietrich WD, Kuluz JW. Traumatic injury activates MAP kinases in astrocytes: mechanisms of hypothermia and hyperthermia. J Neurotrauma 2009;26:1535-1545.
42. Oda Y, Gao G, Wei EP, Povlishock JT. Combinational therapy using hypothermia and the immunophilin ligand FK506 to target altered pial arteriolar reactivity, axonal damage, and blood-brain barrier dysfunction after traumatic brain injury in rat. J Cereb Blood Flow Metab 2011;31:1143-1154.
43. Hatic H, Kane MJ, Saykally JN, Citron BA. Modulation of transcription factor Nrf2 in an in vitro model of traumatic brain injury. J Neurotrauma 2012;29:1188-1196.
44. Huang L, Coats JS, Mohd-Yusof A et al. Tissue vulnerability is increased following repetitive mild traumatic brain injury in the rat. Brain Res 2013;1499:109-120.
45. Gu X, Wei ZZ, Espinera A et al. Pharmacologically induced hypothermia attenuates traumatic brain injury in neonatal rats. Exp Neurol 2015;267:135-142.
46. Lee JH, Wei L, Gu X, Wei Z, Dix TA, Yu SP. Therapeutic effects of pharmacologically induced hypothermia against traumatic brain injury in mice. J Neurotrauma 2014;31:1417-1430.
47. Lotocki G, de Rivero Vaccari JP, Perez ER et al. Alterations in blood-brain barrier permeability to large and small molecules and leukocyte accumulation after traumatic brain injury: effects of post-traumatic hypothermia. J Neurotrauma 2009;26:1123-1134.
48. Doll H, Maegele M, Bohl J et al. Pharyngeal selective brain cooling is associated with reduced CNS cortical lesion after experimental traumatic brain injury in rats. J Neurotrauma 2010;27:2245-2254.
49. Fujita M, Wei EP, Povlishock JT. Effects of hypothermia on cerebral autoregulatory vascular responses in two rodent models of traumatic brain injury. J Neurotrauma 2012;29:1491-1498.
50. Miyauchi T, Wei EP, Povlishock JT. Evidence for the therapeutic efficacy of either mild hypothermia or oxygen radical scavengers after repetitive mild traumatic brain injury. J Neurotrauma 2014;31:773-781.
51. Szczygielski J, Muller A, Mautes AE et al. Selective brain hypothermia mitigates brain damage and improves neurological outcome after post-traumatic decompressive craniectomy in mice. J Neurotrauma 2017;34:1623-1635.
52. Feala JD, Abdulhameed MD, Yu C et al. Systems biology approaches for discovering biomarkers for traumatic brain injury. J Neurotrauma 2013;30:1101-1116.
53. Kell DB, Oliver SG. Here is the evidence, now what is the hypothesis? The complementary roles of inductive and hypothesis-driven science in the post-genomic era. Bioessays 2004;26:99-105.
54. Garland P, Broom LJ, Quraishe S et al. Soluble axoplasm enriched from injured CNS axons reveals the early modulation of the actin cytoskeleton. PLOS ONE 2012;7:e47552.
55. Salehi A, Zhang JH, Obenaus A. Response of the cerebral vasculature following traumatic brain injury. J Cereb Blood Flow Metab 2017;37:2320-2339.
56. Thelin EP, Frostell A, Mulder J et al. Lesion size is exacerbated in hypoxic rats whereas hypoxia-inducible factor-1 alpha and vascular endothelial growth factor increase in injured normoxic rats: a prospective cohort study of secondary hypoxia in focal traumatic brain injury. Front Neurol 2016;7:23.
57. Thelin EP, Jeppsson E, Frostell A et al. Utility of neuron-specific enolase in traumatic brain injury; relations to S100B levels, outcome, and extracranial injury severity. Crit Care 2016;20:285.
58. Thelin EP, Just D, Frostell A et al. Protein profiling in serum after traumatic brain injury in rats reveals potential injury markers. Behav Brain Res 2016. https://doi.org/10.1016/j.bbr.2016.08.058.
59. Yang DB, Yu WH, Dong XQ et al. Serum macrophage migration inhibitory factor concentrations correlate with prognosis of traumatic brain injury. Clin Chim Acta 2017;469:99-104.
60. Sharma R, Rosenberg A, Bennett ER, Laskowitz DT, Acheson SK. A blood-based biomarker panel to risk-stratify mild traumatic brain injury. PLOS ONE 2017;12:e0173798.